JOURNAL OF MATERIALS SCIENCE 31 (1996) 252–261

Dynamic consolidation/hot isostatic pressing of SiC

S.-S. SHANG, M. A. MEYERS
Dept. of Applied Mechanics and Engineering Sciences and Institute for Mechanics and Materials, University of California, San Diego, La Jolla, CA 92093, USA

Shock consolidation is a method that presents a bright potential but has been limited by inevitable cracking of compacts, especially for ceramics. In an effort to eliminate cracking while retaining the unique features of shock consolidation, three novel approaches have been implemented: (1) the use of local shock-induced reactions to increase the temperature of particle surfaces and to provide a bonding phase (reaction products); (2) shock densification at a low pressure (just above the threshold for pore collapse) followed by hot isostatic pressing; (3) shock consolidation of pre-heated specimens. These techniques were applied to silicon carbide. Reduction of cracking was observed with interparticle melting and reactions. Microstructural results, mechanical properties and advantages and limitations of these approaches are discussed. It is shown that shock consolidation of ceramics is inherently limited because shock-induced cracks are introduced into the process, damaging the particles. A criterion for the plastic deformation versus fracture of ceramic powders under shock consolidation is proposed.

1. Introduction

Silicon carbide, a non-oxide ceramic, has excellent mechanical properties at elevated temperatures but it is very difficult to sinter. It is customary to use sintering aids in the sintering process of silicon carbide [1]. However, the presence of sintering aids deteriorates the mechanical strength at high temperature. Production of dense sintered compacts without any sintering aids has not yet been successful to date. The dynamic compaction process has potential to produce compacts without sintering aids. However, there still remain some serious problems in applying dynamic compaction to actual ceramic processing: macrocracks and remaining pores are the two major problems in the dynamic consolidation of silicon carbide powders [2]. Macrocracks are caused by both geometrical constraints due to shock-wave reflection, and excess energy due to the high velocity of impact. In high-hardness, low-toughness materials, the critical flaw sizes are small, whereas the pressures required for consolidation are high [3]. Thus, it is very difficult to obtain crack-free compacts of these materials. Low shock pressures, preheating the powders and post-shock heat treatment have been suggested as possible methods to alleviate these problems [4, 5]. Particle size, particle-size distribution, and trapped gas are all believed to play an important role in ceramic processing. The objective of this investigation was to develop a procedure to produce monolithic SiC without additives which decrease their high-temperature capability. Thus, dynamic densification was used either alone or in combination with post-shock sintering or hot isostatic pressing (HIPing) in an attempt to produce bulk SiC from powder. Elemental mixtures of silicon and carbon were also added to SiC powders in order to aid the consolidation through a reaction leading to the synthesis of SiC.

2. Experimental procedure

Two experimental shock systems, the "Sawaoka" fixture [6] and the double-tube (cylindrical) fixture, were used in this investigation. The Sawaoka fixture (Fig. 1) was used for one-step shock consolidation, because it provides, through the high impact velocity of the flyer plate, an energy level sufficient for interparticle melting. The high-temperature arrangement for this fixture was developed by Yu and Meyers [7]. The powder is preheated to the proper temperature in the furnace and then the flyer plate with explosive slides down to the assembly by activating a solenoid. The planar impact of the flyer plate on the system creates high amplitude shock waves that are transmitted through the powders. The detonation is initiated from the detonator at the top of the apparatus. The conical lens (plane wave generator) consists of explosives with two detonation velocities and generates a planar wave in the main charge. The flyer plate is accelerated by the main charge and impacts the capsules, consolidating the powders. The fixture and capsules have to retain sufficient integrity after being shock loaded to enable recovery of the consolidated material used. After an unsuccessful experiment using stainless steel capsules, Inconel 718 was used to contain the specimens. The impact velocity in those experiments was 2000 $m\,s^{-1}$, yielding an estimated presence (one-dimensional) of 12 GPa.

The cylindrical double-tube [8] fixture (Fig. 2) was used for densification followed by hot isostatic

0022–2461

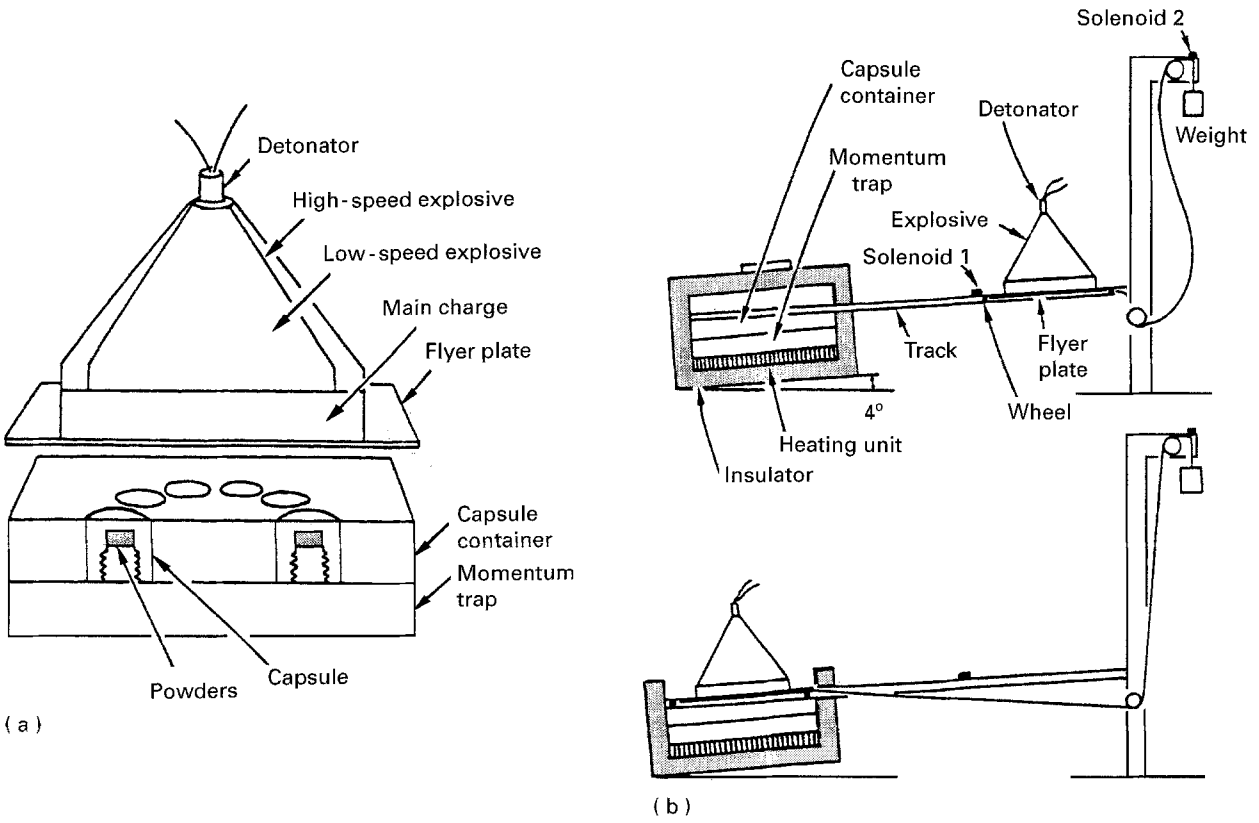

Figure 1 Schematic illustrations of (a) the planar impact system, and (b) the hot consolidation apparatus.

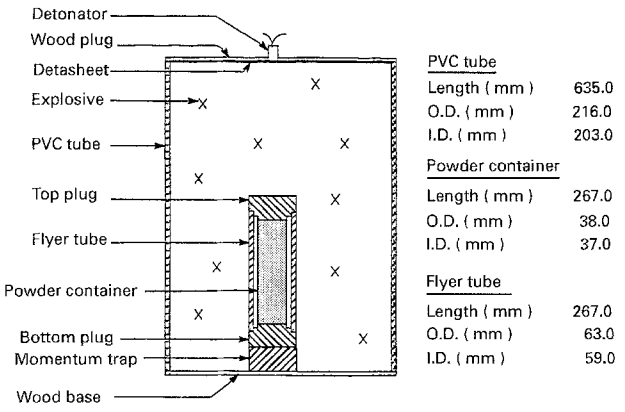

Figure 2 Cylindrical axisymmetric double-tube system and its experimental dimensions for cylindrical geometry.

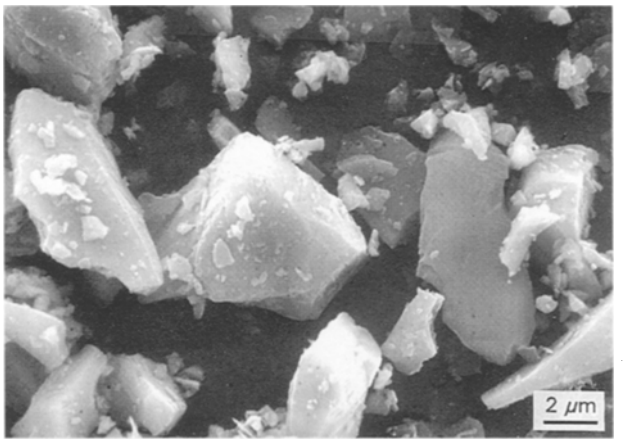

Figure 3 Scanning electron micrograph of unshocked 7 μm SiC powder.

pressing/sintering as well as shock consolidation. The larger specimens provided by this method are much better suited for subsequent mechanical testing. This technique generates pressures in the powder that can be several times higher than those generated without a flyer tube [8]. The explosive charge is contained in a PVC plastic tube resting on a wooden base and surrounds a mild steel flyer tube, in the centre of which is the assembly containing the powder (stainless steel pipe with top and bottom steel plugs). The shock pressure can be varied widely and easily by changing the type and quantity of explosive used. Detasheet (a plastic explosive in sheet form) is used to create a more uniform detonation front. The explosion is initiated at the top and causes the implosion of the tube containing the powder, as the detonation front moves downward. The estimated impact velocity in the experiments conducted was 1700 $m\,s^{-1}$, yielding a pressure in the powder of 9 GPa (one-dimensional calculation).

3. Results and discussion

3.1. Dynamic consolidation of SiC with a high-temperature planar impact system

Two different sizes of pure SiC powders (7 and 44 μm) were used as starting materials. Fig. 3 shows that the morphology of 7 μm SiC powder is highly irregular. The SiC powders were supplied by CERAC, Milwaukee, WI. The high-temperature planar impact system developed by Yu and Meyers [7] was used for

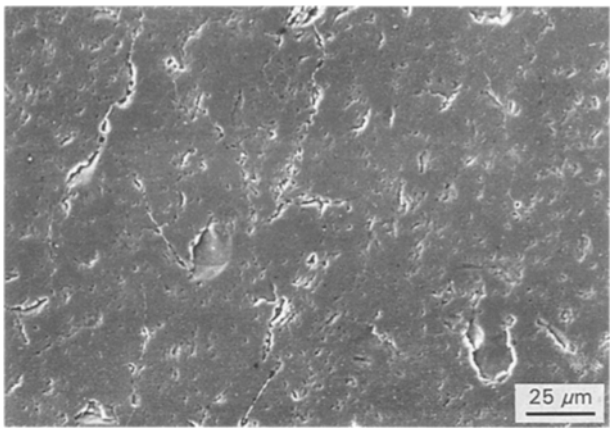

Figure 4 Scanning electron micrograph of the polished surface of consolidated 44 μm SiC compacts.

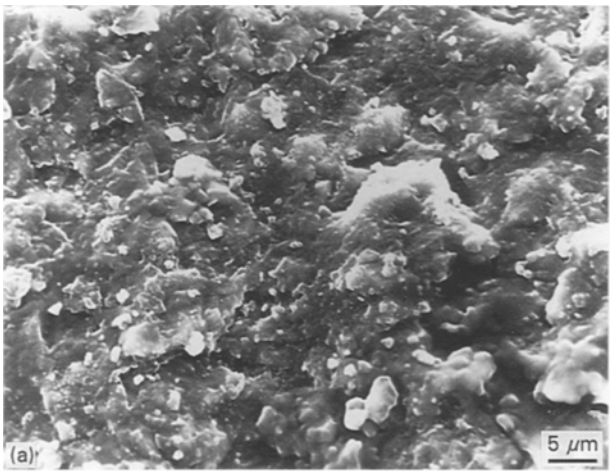

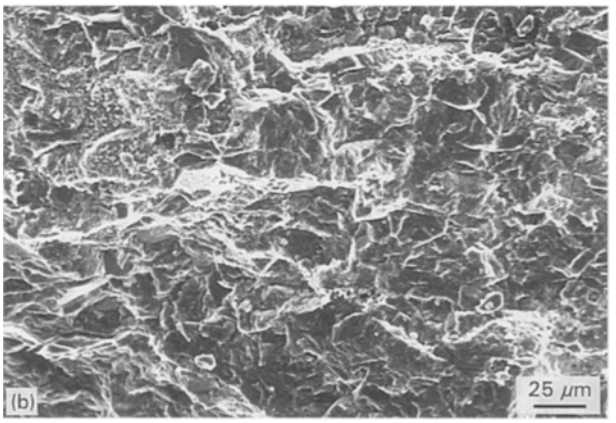

Figure 5 Scanning electron micrograph of the fracture surface of consolidated (a) 7 μm and (b) 44 μm SiC.

the consolidation. Well-consolidated samples were obtained upon shocking preheated SiC powders with 65% theoretical density at the impact velocity of 2 km s^{-1} (12 GPa pressure). It should be noticed that three-dimensional computations predict significantly higher pressures [9]. Cracking, prevalent in ambient temperature shock consolidation, is not totally eliminated and circumferential cracks are noticeable. Scanning electron microscopic (SEM) analysis (Fig. 4) of recovered 44 μm SiC compacts revealed that SiC particles underwent a considerable amount of deformation and the material was fully densified. Fig. 5a

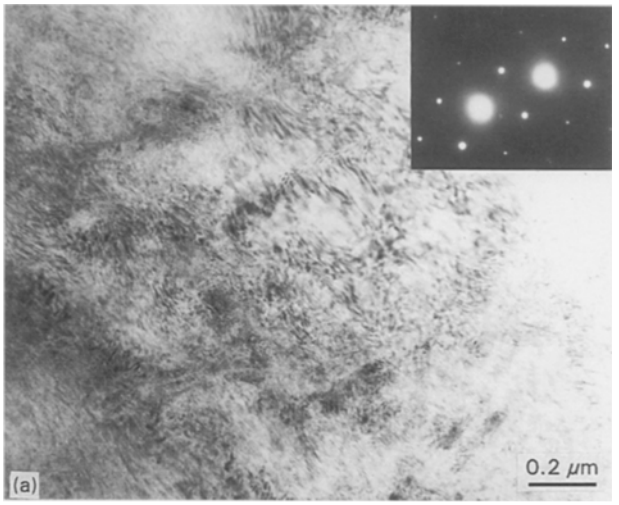

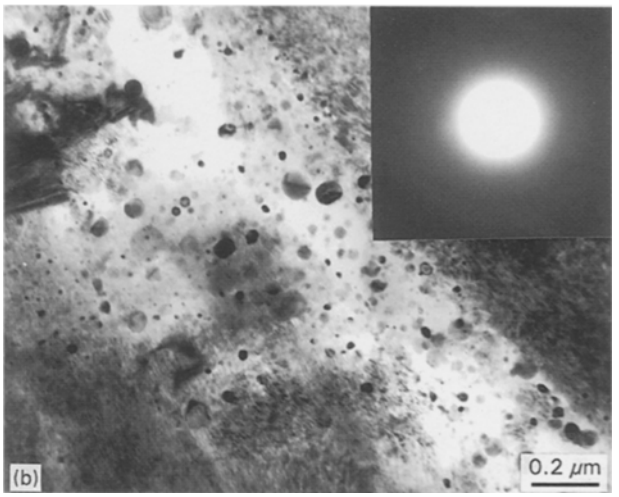

Figure 6 Transmission electron micrographs of consolidated 44 μm SiC showing (a) lattice distortion in the interior of SiC particle, and (b) the surface layer in the interparticle region.

and b showed microstructures of fracture surfaces of 7 and 44 μm SiC compacts, respectively. Both fractographs indicate that cracks are transgranular and this is evidence for the excellent bonding of the powders. The relative densities of the 7 and 44 μm SiC compacts were 98.8% and 98.5% theoretical, respectively. Both samples had a very close average microhardness value of 28 GPa. Transmission electron microscopic (TEM) analysis (Fig. 6) revealed the substructural features of the 44 μm SiC compacts. Lattice distortion in the interior of an SiC particle can be observed, indicating that the particle was heavily deformed (Fig. 6a). Fig. 6b shows the interparticle region. The dark round regions (8–80 nm) in the micrograph are nanocrystalline SiC particles, while the white surrounding material corresponds to an amorphous phase. This interfacial layer was formed due to the very rapid collapse of the gaps between the particles as well as the rapid deposition of energy upon interparticle sliding. This ultra-rapid deformation and energy deposition produce melting or sublimation at the particle surfaces followed by a rapid solidification via heat conduction into the interior of the particles. Furthermore, this thin surface layer (0.2–0.3 μm) and high thermal

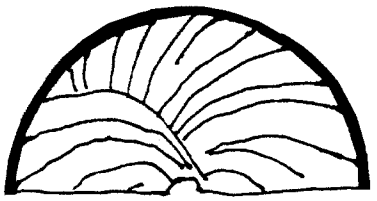

(b)

Figure 7 Scanning electron micrographs showing (a) the microstructures of the 7 μm SiC + Si + C alloy, (b) traces of shear localization regions.

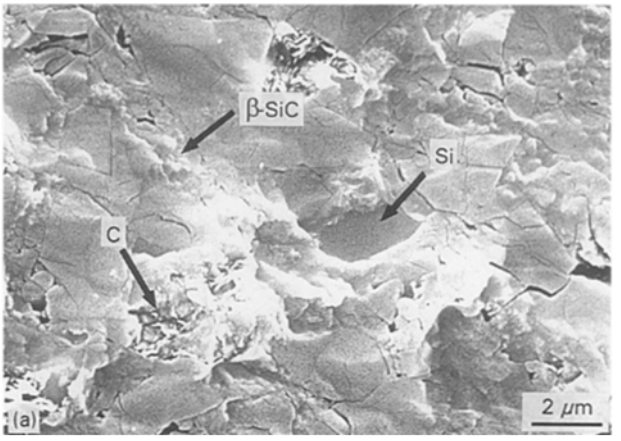

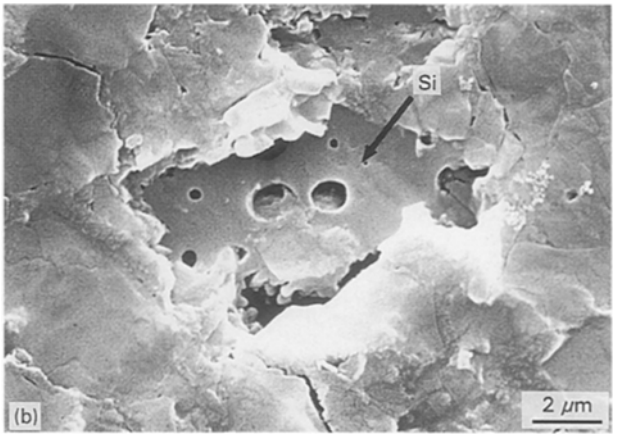

Figure 8 Scanning electron micrographs of (a) consolidated 7 μm SiC + Si + C alloy from the matrix, (b) silicon which was melted and then resolidified after compaction.

conductivity of SiC (13 $W m^{-1} °C^{-1}$) also promote the tendency for these nanocrystalline structure and amorphous phase. This energy deposition time is of the order of the wave transit time through the particle (a few nanoseconds) [10]. The melted or sublimated interparticle material resolidifies at cooling rates as high as 10^5–10^{10} $K s^{-1}$ [11]. It is believed that amorphous SiC phase forms at a higher cooling rate than nanocrystalline structure and that the crystalline phase nucleates within the amorphous region while it is being cooled. However, another possibility is that melted or sublimated SiC reacted with oxygen to form $Si_xC_yO_z$ or SiO_2 which also has the tendency to form an amorphous phase. Incontrovertible identification was not possible by transmission electron microscopy.

3.2. Dynamic consolidation of SiC + Si + C with the cylindrical impact system

Pure SiC powders (7 and 44 μm) admixed with 13 wt % Si and 5.6 wt % C were used as starting materials in this cylindrical impact system. This proportion of elemental powders provides the stoichiometric composition SiC. The green compacts were impacted by a stainless steel flyer tube at an impact velocity of 1700 $m s^{-1}$ (9 GPa pressure). A first experiment using an impact velocity of 1200 $m s^{-1}$ did not succeed in bonding the powders. SEM images of recovered 7 μm SiC + Si + C compacts (Fig. 7) showed that material was fully densified. The profuse formation of helicoidal (or spiral) shear bands was observed in the compacts. Scanning electron microscopic analysis of the material from the matrix (Fig. 8) revealed that silicon and carbon particles underwent a considerable amount of deformation. SiC particles are very brittle and are subject to bending moments due to their highly irregular shape. Thus, profuse microcracks were observed in the interior of the SiC particles. The particulates with smooth and crack-free surfaces (marked in the figure) correspond to unreacted silicon and the dark needle-like particulates correspond to unreacted carbon (arrow C in Fig. 8a), while very fine particles (0.3–0.5 μm) in the image (marked in the figure) correspond to the reaction products of silicon and carbon. Spherical voids were observed in the silicon particles (Fig. 8b), indicating that some silicon particles, upon compaction, melted and then resolidified. When the molten silicon resolidifies, the entrapped gases expand and form spherical voids which minimize the surface area.

The material within the shear localization regions showed a somewhat different microstructure from that of the matrix. It should be noticed that this is the first report of a shear localization region in which chemical reaction was triggered. It is based on observations by Meyers and Yu [12]. The temperature rise produced by intense plastic deformation was sufficient to initiate the reaction, whereas the shock wave in the surrounding material did not effect the reaction. Scanning electron microscopic analysis of the material from these shear bands revealed that the reacted material consists of very fine grains, ranging between 0.3 and 0.5 μm (Fig. 9a and b). These fine grains are

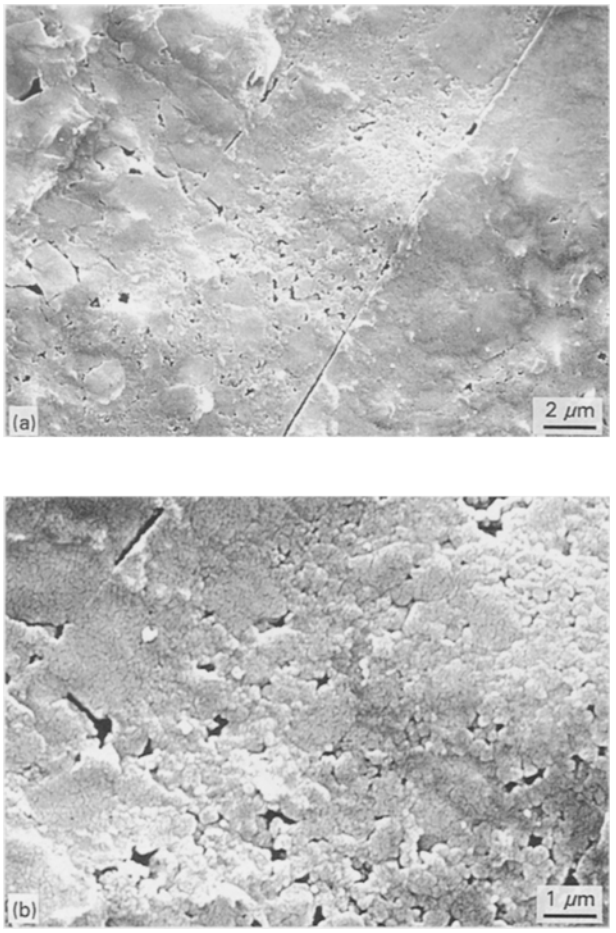

Figure 9 Scanning electron microscopic analysis from (a) a shear band showing that the shear band consists of very fine grains (0.3–0.5 μm); (b) high magnification from (a).

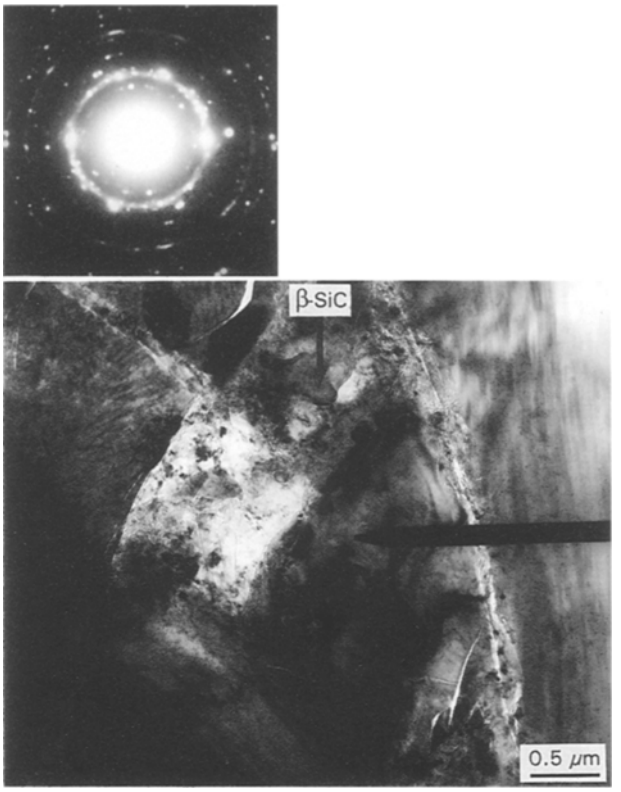

Figure 10 Transmission electron micrograph of 7 μm SiC + Si + C after dynamic consolidation showing dislocations and microcracks in the SiC.

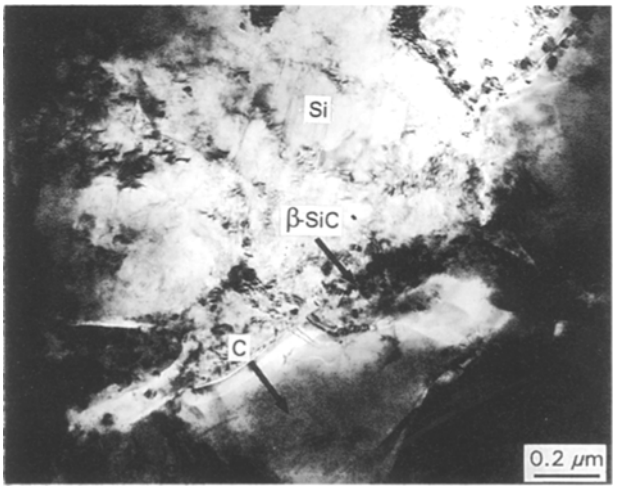

Figure 11 Transmission electron micrograph showing localized deformation and partial chemical reaction in the silicon and carbon mixture.

believed to be the product of reaction between silicon and carbon powders. The matrix and the band are clearly divided by a rather distinct interface. These bands are believed to be the preferential paths for plastic deformation as the shock front propagates towards the cylinder axis. It is believed that this shear localization phenomenon occurs along the softer materials silicon and carbon due to their much lower strength. The trajectory of these bands corresponds to the trace of the maximum shear stress, enhancing the exothermic reaction between silicon and carbon. Meyers and Wang [8] analysed the stress state produced by the implosion of a cylinder and were able to explain the formation of these shear localization regions.

Transmission electron microscopic analysis from 7 μm SiC + Si + C compacts showed that the three components were highly deformed and filled the previously existing 35% interparticle voids (Fig. 10a). Dislocations in high densities and microcracks were observed in the interior of the SiC particles. The reaction product between silicon and carbon (marked in the figure) was identified to be 0.3–0.5 μm β-SiC, whereas the matrix particles have the α (hexagonal) structure. The selected-area diffraction pattern clearly shows the microcystalline β structure (Fig. 10) because of the ring pattern in which a number of grains are simultaneously diffracted. This microcrystalline structure seems to be free from deformation, possibly due to recrystallization after the passage of the shock wave. Relative movement between SiC particles appeared to be the dominant factor determining the microstructural features and dislocation density in SiC particles. The transmission electron micrograph (Fig. 11) shows the localized deformation and partial chemical reaction in the silicon and carbon mixture (marked in the figure). Unreacted silicon with a high density of dislocations and deformation twins in weak contrast are observed. Unreacted carbon seems to have less deformation than silicon and original α-SiC.

Localized reactions were found at the interface between silicon and carbon (marked in the figure). Relative mass motion, plastic flow and contact surface between particles are considered to play an important role in chemical reactions, but the mechanism is not well understood. Graham *et al.* [13] advanced the concept of CONMAH (configuration, mixing, activation and heating) that provides some guidelines regarding the unique processes happening of the shock front during chemical reaction.

3.3. Dynamic consolidation of SiC with the cylindrical impact system

The starting powder sizes used in this cylindrical consolidation configuration were 7 and 44 μm SiC. Two impact velocities, 1.2 and 1.7 km s^{-1}, were employed. According to the one-dimensional impedance match technique, the shock pressures are 6 and 10 GPa, respectively. The 44 μm SiC powder after dynamic consolidation was observed to be very unconsolidated. Most of the sample was loose powder. Particle fracture was observed in the resulting compacts. Generation of particle fracture usually reduces the energy dissipation (plastic deformation) on the surface to form fused compacts. Furthermore, the cylindrical impact system creates a lower shock pressure in the powder, as compared with the planar impact system. This lower shock pressure could not densify the fragments of SiC produced from particle fracture. In contrast, a well-densified sample from 7 μm SiC was obtained. Particle fracture was also observed in the sample. The interstitial void volume of 7 μm SiC is smaller than that of 44 μm. Potter and Ahrens [14] obtained similar results for diamond powder. Particle fracture is not a dominant mechanism for densification. It is believed that 7 μm SiC powders were densified by both plastic deformation and particle fracture. This aspect is discussed in detail in Section 3.5.

3.4. Hot isostatic pressing of dynamically densified SiC powder

Following the dynamic densification process, samples were HIPed at 1873 and 2223 K for 2 h. The temperatures were chosen because they are higher than the melting point of silicon; the major reaction between silicon and carbon can proceed at a higher rate. The pressure, 200 MPa, was applied in an argon atmosphere. Scanning electron microscopic analysis of the sample (7 μm SiC + Si + C) recovered from HIPing at 1873 K revealed porosity in the reaction region, residual hair-like silicon, and plate-like carbon (Fig. 12). There is a considerable degree of reaction induced by the HIPing process. This hair-like residual silicon is usually found in the large gaps between original SiC powders. These porosities are believed to be shrinkage that occurred when silicon and carbon reacted. The HIPed pressure is not sufficiently large to collapse the shrinkage. This factograph revealed failure via a transgranular mode from original α-SiC and intergranular

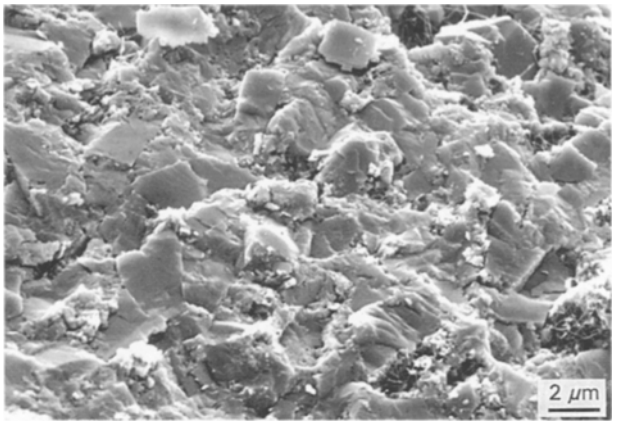

Figure 12 Fractographs from the fracture surface of consolidated 7 μm SiC + Si + C after 1600 °C HIPing

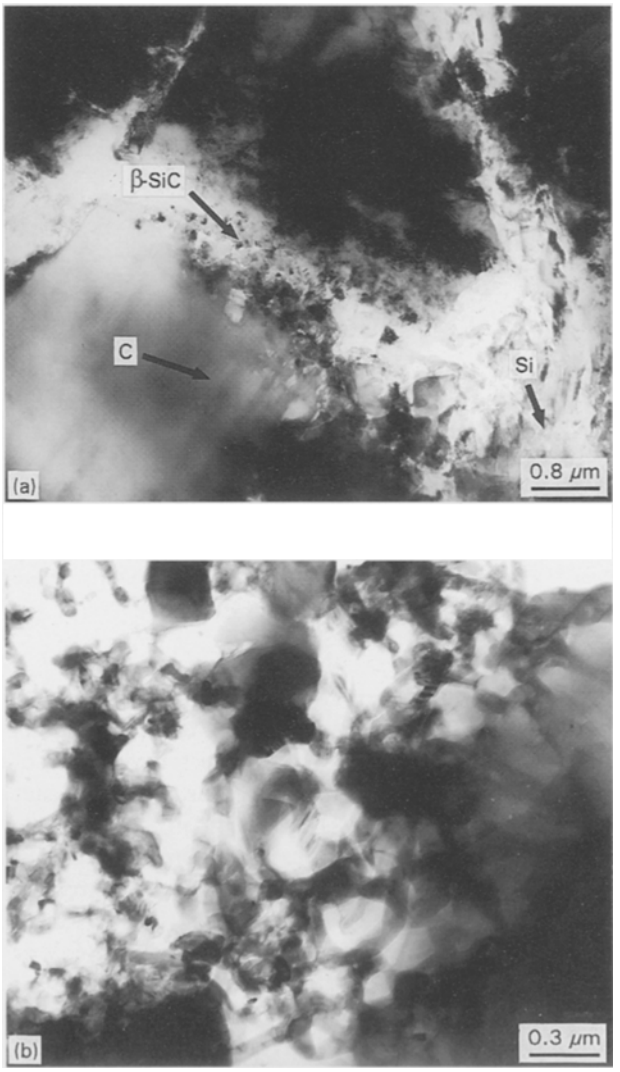

Figure 13 Transmission electron micrographs of (a) shock densified 7 μm SiC + Si + C after 1600 °C HIPing showing localized partial reaction region of solid C and liquid Si; (b) resolidification of molten silicon after 1600 °C HIPing.

mode from interparticle regions (β-SiC + Si + C). Transmission electron microscopy revealed the localized reactions in the interparticle regions. Fig. 13a shows the partial reaction region of solid carbon and liquid silicon. These microcrystalline regions were identified to be 0.5 μm β-SiC (cubic) by analysing the

Figure 14 Transmission electron micrograph of shock-densified 7 μm SiC + Si + C after 1600 °C HIPing showing high dislocation densities within carbon grains.

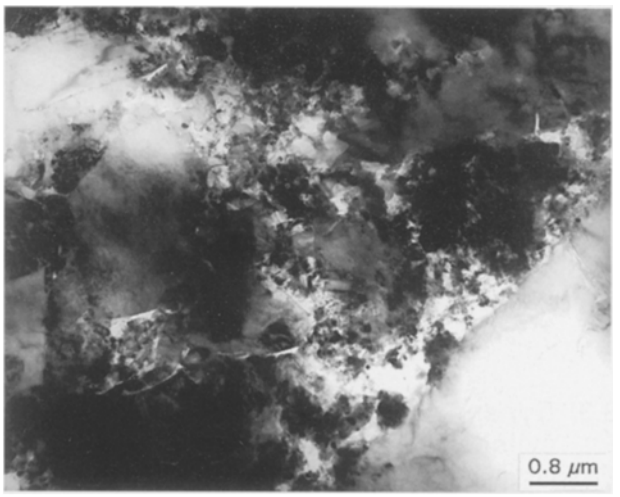

Figure 16 Transmission electron micrograph of shock-densified 7 μm SiC + Si + C after 1950 °C HIPing showing more reaction product (β-SiC) observed in the interparticle region.

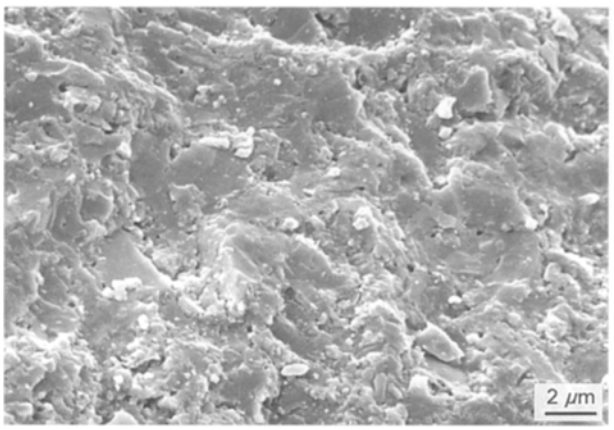

Figure 15 Scanning electron micrograph of a fracture surface from shock-densified 7 μm SiC + Si + C after 1950 °C HIPing.

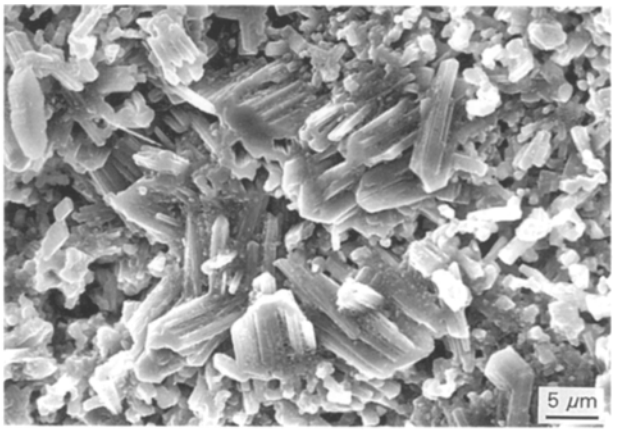

Figure 17 Fractographs from the fracture surface of shock-densified 7 μm SiC after 1950 °C HIPing.

selected-area diffraction pattern. Resolidification of molten silicon was observed in the interstitial regions (Fig. 13b). This is probably because the viscosity of liquid silicon is still high at 1873 K for silicon to react with carbon. Transmission electron microscopy revealed significant dislocation densities within carbon grains (Fig. 14) due to its much lower strength and associated higher deformation. The average microhardness value of the 1873 K HIPed sample was approximately 14.8 ± 5 GPa. A significant amount of variation shown in the microhardness value is due to the residual silicon and carbon and intergranular voids.

Analysis of the material (7 μm SiC + Si + C) recovered after HIPing at 2223 K (Fig. 15) revealed that the reaction products bonded the SiC much better, as compared to the compacts produced using HIPing at 1873 K. The viscosity of silicon is quite high at 1873 K but falls at 2223 K. Therefore, it wets the carbon and silicon carbide more easily and enhances the exothermic reaction (silicon and carbon). This local temperature rise increases the solubility of the graphite in the silicon resulting in further dissolution. Intergranular void volume was tremendously decreased and residual unreacted silicon was also much less than in the 1873 K HIPed sample. Ness and Page [15] found that the fine β-SiC in liquid silicon has the tendency to migrate and overgrow on to the surface of an α-SiC. This is because the dissolved graphite prefers to diffuse to locally cooler nucleation sites (original α-SiC) and reacts with silicon. The β-polytype SiC overlayer grows along the external surface of α-SiC and has various microstructural features: fully or partially $\beta \rightarrow \alpha$ transformed epitaxial coating. Transmission electron microscopy studies of 1873 K HIPed 7 μm SiC + Si + C (Fig. 16) revealed more reacted product (β-SiC) observed in the interparticle region. The formation and migration of β-SiC confirms Ness and Page's [15] observations.

Well-densified 7 μm SiC (without Si + C addition) was HIPed at 2223 K for 2 h. Scanning electron microscopy of the fracture surface is shown in Fig. 17. The microstructure of the 2223 K HIPed SiC appears to have two grain morphologies i.e. 10–15 μm randomly elongated and 1–4 μm equiaxed. The transmission electron micrograph in (Fig. 18) shows that HIPing annealed out the lattice distortion in the interior of SiC powders. This is typical of the HIPing process

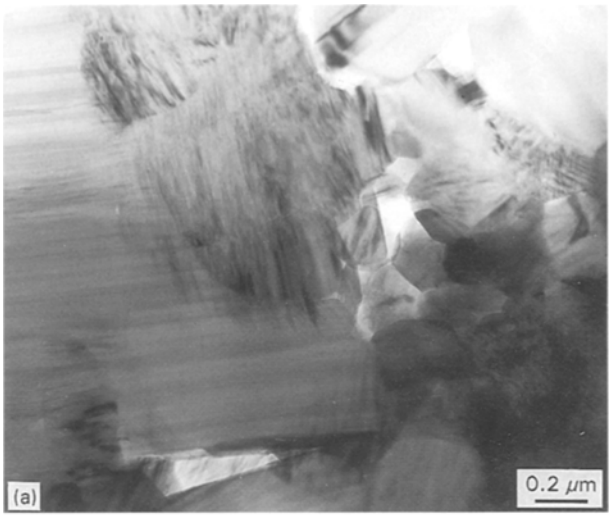

Figure 18 Transmission electron micrograph of shock-densified 7 μm SiC after 1950 °C HIPing.

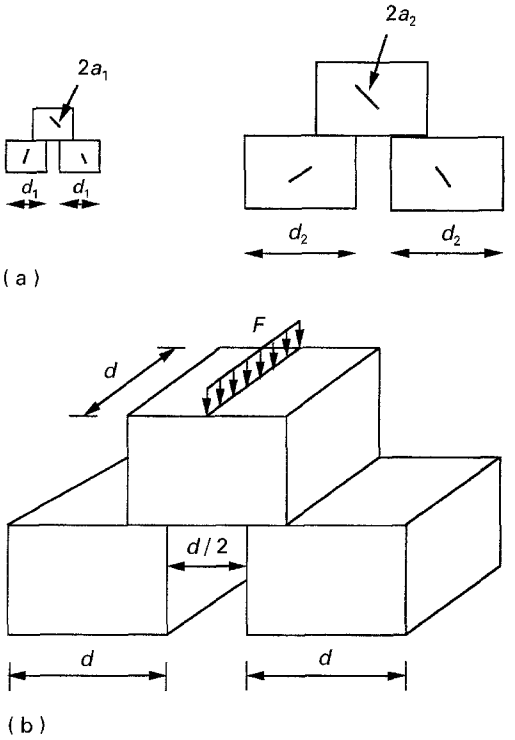

Figure 19 Schematic representation of ceramic powder as cubical particles stacked in a simple arrangement: (a) particle size–crack size effects; (b) loading and dimensions.

where high temperatures and hold times result in strain-free crystals. One can also notice the presence of 0.1–0.8 μm equiaxed grains. One possible explanation for this observation is that the equiaxed grains formed as a result of grain growth of fractured or originally small particles during the HIPing process. Intergranular voids with diameters of the order of 0.2 μm were observed. This indicates that residual intergranular voids after dynamic processing could not be completely collapsed during the HIPing process. Another interesting feature is the presence of amorphous and microcrystalline phase (see Fig. 6b) found along the grain boundaries. This is evidence of plastic deformation or friction from crystal-boundary sliding in SiC. The average microhardness of the 1873 K HIPed 7 μm SiC was approximately 26.0 ± 2 GPa which is comparable to hot-pressed SiC (27 GPa). The mechanical strength of this silicon carbide was determined and compared with commercially available hot-pressed and sintered silicon carbide (Cercom, Vista). The average compressive strength of the shock/hip SiC was approximately 300–500 MPa. The compressive strength of the hot-pressed SiC was approximately 1.5–2.1 GPa and approximately 1.2–1.6 GPa for sintered silicon carbide. The lower compressive stress of the shock/hip SiC was a result of the residual macrocracking.

3.5. Particle-size effects

The greater tendency for larger particles to undergo fracture while smaller ones plastically deform was previously reported by Akashi and Sawaoka [16] and Potter and Ahrens [14] for diamond powders. A possible interpretation for the particle-size dependence of the mechanism of packing is the following: larger particles contain a greater number of flaws (flaw density being constant, the number of flaws per particle increases with the cube of the volume) than smaller particles (Fig. 19a). Thus, smaller particles deform plastically, whereas larger particles fragment under the effect of shock pressures. The greater tendency for larger particles to undergo fracture while smaller ones plastically deform was previously reported by Akashi and Sawaoka [16] and Kondo and Sawai [17–19], for diamond powders. The analysis below shows that this is the direct effect of the tensile stresses generated by bending and shear. These stresses activate the flaws existing in the powders, fragmenting them. Smaller particles have, necessarily, smaller flaws (the maximum flaw size, $2a$, being equal to the particle size, d) and the particles, as a result, flow plastically in response to the stresses (compressive, tensile, and shear) generated by the pressure pulse. Fig. 19 shows a schematic arrangement of powders as a stacking of cubes. The stresses generated by the application of the external stress pulse are very complex and vary temporally and spatially. Nevertheless, the simplified

analysis below provides an assessment of the stress levels within the particles. The cuboidal particles having a side equal to d, the maximum tensile stress produced by the application of a force F is

$$\sigma = \frac{MdR}{2D} \quad (1)$$

M is the bending moment and I is the moment of inertia. Taking

$$M = \frac{Fd}{4} \quad (2)$$

$$I = \frac{d^4}{12} \quad (3)$$

$$\sigma = \frac{3F}{2d^2} \quad (4)$$

the shear stresses can be approximated as

$$\tau = \frac{F}{d^2}$$

The applied force, F, is related to the pressure, P, by

$$F = k_1 d^2 P \quad (5)$$

where k_1 is a geometrical factor and is dependent on the porosity and number of contact points. It is in the range $0.5 < k_1 < 2$. Thus, the maximum stress, σ, from Equations 4 and 5 is

$$\sigma = \frac{3}{2} k_1 P \approx P \quad (6)$$

The effect of the tensile stress, σ, on an existing flaw of size $2a$ is

$$K_{IC} = k_2 \sigma (\pi a)^{1/2} \quad (7)$$

K_{IC} is the fracture toughness of the material and k_2 is a factor incorporating the boundary conditions and flaw geometry.

Substituting Equations 4 and 5 into Equation 7

$$a = \frac{1}{\pi}\left(\frac{2K_{IC}}{3k_2 k_1 P}\right)^2 \quad (8)$$

it is possible to estimate the critical flaw size (flaw that will be activated) for a certain material, at a prescribed pressure level. For SiC, the flyer tube geometry provides a pressure, P, that is approximately 10 GPa. The fracture toughness of SiC is $\sim 5\ \mathrm{MN\,m^{-3/2}}$. Equation 8 provides, assuming $k_1 = k_2 = 1$, $a = 3 \times 10^{-9}$ m. This corresponds to a flaw size of 6 nm. This value is much lower than the particle sizes (7–44 μm) and, therefore, the fracture/plastic deformation transition is not determined by flaw size, but by the availability of flaws. Three factors are considered important in determining the flaw population within a ceramic: density of flaws, size distribution of flaws, and orientation distribution of flaws.

The distribution of flaws in a ceramic can be described by the cumulative function [20]

$$N_c = N_0 e^{(-a_c/a_i)} \quad (9)$$

where N_c is the number of flaws per unit volume greater than a_c, N_0 is the total number of flaws per unit volume, and a_i is a functional dependence. By substituting Equation 7 into Equation 9

$$N_c = N_0 e^{-K_{IC}^2/\pi k_2^2 \sigma_{a_i}^2} \quad (10)$$

The local requirement for fracture is that a flaw of sufficient size and appropriate orientation is present, such that it can be activated by the local stress fields. The stress fields within the particles are highly non-uniform but it is possible, through simple assumptions, to arrive at a fairly realistic description. The following assumptions will be made: (a) flaw orientations are neglected, (b) stress in particles is assumed to be constant. An average tensile stress is taken as $3P/2$, threehalves the maximum tensile stress in the particles (Equation 6). The volume of each particle being d^3, it will fracture if it contains one or more flaws of supercritical size. This corresponds, in Equation 10 to

$$N_0 d^3 \exp\left(-\frac{4K_{IC}^2}{\pi k_2^2 a_i P^2}\right) = 1 \quad (11)$$

Expressing Equation 11

$$d = \exp\left(\frac{4K_{IC}^2}{\pi k_2^2 a_i P^2}\right) \Big/ N_0^{1/3} \quad (12)$$

Equation 12 gives the maximum size of particles that undergo plastic deformation. This occurs when the particle has at least one supercritical flaw. Pre-shock preparation of the particles can significantly affect N_0 and a_i, the parameters that describe the distribution of flaws; therefore, the maximum particle size is critically dependent on processing.

4. Conclusion

Two experimental configurations were used for the SiC shock experiments: the Sawaoka high-temperature and the cylindrical double-tube configuration. In the double-tube configuration, silicon carbide powder of two sizes (44 and 7 μm) with and without the addition of the elemental mixture Si + C was shock densified and subsequently HIPed at 1873 and 2223 K. The HIPing treatment was intended to complete the Si + C reaction but was only partially successful. The larger particle size SiC (44 μm) underwent extensive microcracking (within the particles) due to the effect of the shock wave, whereas the smaller SiC (7 μm) material consolidated better. The mechanical strength of this silicon carbide was determined and compared with commercially available hot-pressed and sintered silicon carbide (Cercom, Vista). Average compressive strength of the shock/HIP SiC was approximately 300–500 MPa. The compressive strengths for the hot-pressed SiC were approximately 1.5–2.1 GPa and approximately 1.2–1.6 GPa for sintered silicon carbide. The lower compressive stress of the shock/HIP SiC was as a result of the residual macrocracking. In the Sawaoka high-temperature fixture, samples had an average microhardness value of 28 GPa. The interfacial layer was observed at the interparticle regions. In the Sawaoka high-temperature

fixture, the resulting compacts exhibited high integrity, with an interparticle layer that was identified by transmission electron microscopy to be a mixture of amorphous and nanocrystalline SiC. The microhardness was equal to that of conventionally processed SiC: 27–28 GPa.

It has been shown, by means of a calculation, that smaller particles preferentially undergo plastic deformation, whereas larger particles fracture in shock consolidation. These different consolidation mechanisms are due to the availability of supercritical flaws for the larger particle sizes. A criterion for plastic deformation versus fracture of ceramics under shock consolidation, is proposed.

Acknowledgements

This research was sponsored by the National Science Foundation Materials Processing Initiative Awards DMR 8713258 and DMR 91-5835R1. The authors thank Dr K. Hokamoto, Dr Kim, Dr Li-Hsing Yu, and Dr Kenneth Vecchio for their assistance during the work. The use of the facilities of the Center of Excellence for Advanced Materials is gratefully acknowledged. The explosive experiments were carried out at the Center for Explosives Technology Research, New Mexico Tech, Socorro, NM, through the kind assistance of Professor N. N. Thadhani.

References

1. S. SOMIYA, "Advanced Technical Ceramics" (Academic Press, San Diego, 1989) p. 62.
2. T. AKASHI, V. LOTRICH and A. B. SAWAOKA, *J. Am. Ceram. Soc.* **12** (1985) C-322.
3. M. A. MEYERS, S. S. SHANG and H. HOKAMOTO, in "Shock Waves in Materials Science", edited by A. B. Sawaoka (Springer, Tokyo, 1993) p. 145.
4. S. S. SHANG, H. HOKAMOTO and M. A. MEYERS, *J. Mater. Sci.* **27** (1992) 5470.
5. S. S. SHANG and M. A. MEYERS, *Metall. Trans.* **22** (1991) 685.
6. T. AKASHI and A. B. SAWAOKA, US Pat. 4655830 (1987).
7. L. H. YU and M. A. MEYERS, in "Metallurgical Applications of Shock Wave and High- Strain-Rate Phenomena", edited by M. A. Meyers, L. E. Murr and K. P. Staudhammer' (Marcel Dekker, New York, 1992) 303.
8. M. A. MEYERS and S. L. WANG, *Acta Metall.* **4** (1988) 925.
9. F. R. NORWOOD, R. A. GRAHAM and A. B. SAWAOKA, in "Shock Waves in Condensed Matter", edited by Y. M. Gupta (Plenum Press, New York, 1986) p. 837.
10. R. B. SCHWARZ, P. KASIRAJ, T. VREELAND Jr and T. J. AHRENS, *Acta Metall.* **32** (1984) 1243.
11. D. G. MORRIS, *Metall. Sci.* **15** (1981) 116.
12. M. A. MEYERS and L. H. YU, unpublished results.
13. R. A. GRAHAM, B. MOROSIN, E. L. VENTURINI, M. J. CARR and E. K. BEAUCHAMP, in "Metallurgical Applications of Shock Wave and High-Strain-Rate Phenomena", edited by L. E. Murr, K. P. Staudhammer and M. A. Meyers (Marcel Dekker, New York, 1986) p. 1005.
14. D. K. POTTER and T. J. AHRENS, *Appl. Phys. Lett.* **51** (1987) 317.
15. J. N. NESS and T. F. PAGE, *J. Mater. Sci.* **21** (1986) 1377.
16. T. AKASHI and A. B. SAWAOKA, *ibid.* **72** (1989) 837.
17. S. SAWAI and K. KONDO, *J. Am. Ceram. Soc.* **73** (1990) 2428.
18. K. KONDO and S. SAWAI, *ibid.* **73** (1990) 1983.
19. *Idem* in "Science and Technology of New Diamonds", edited by S. Saito, O. Fukunaga and M. Yoshikawa (KTK, Tokyo, 1990) p. 245.
20. D. R. CURRAN, L. E. SEAMAN and D. A. SHOCKEY, in "Shock Waves and High-Strain-Rate Phenomena in Metals", edited by M. A. Meyers and L. E. Murr (Plenum, New York, 1981) p. 129.

Received 17 December 1993
and accepted 7 June 1995